Photoinduced electron transfer at liquid/liquid interfaces Part II. A study of the electron transfer and recombination dynamics by intensity modulated photocurrent spectroscopy (IM...

ARTICLE *in* PHYSICAL CHEMISTRY CHEMICAL PHYSICS · APRIL 1999

Impact Factor: 4.49 · DOI: 10.1039/a900142e

PCCP

Photoinduced electron transfer at liquid/liquid interfaces

Part II.† A study of the electron transfer and recombination dynamics by intensity modulated photocurrent spectroscopy (IMPS)

David J. Fermín, H. Dung Duong, Zhifeng Ding, Pierre-François Brevet and Hubert H. Girault*

Laboratoire d'Electrochimie, Departement de Chimie, Ecole Polytechnique Fédérale de Lausanne, CH-1015 Lausanne Switzerland. E-mail: Hubert.Girault@epfl.ch; Fax: + 41 21 693 3667

Received 5th January 1999, Accepted 9th February 1999

The dynamics of photoresponses associated with heterogeneous quenching of zinc tetrakis(carboxphenyl)porphyrin (ZnTPPC) and ferrocene derivatives at the water/1,2-dichloroethane interface were studied by intensity modulated photocurrent spectroscopy (IMPS). The contribution arising from the electron injection, recombination–product separation competition and the attenuation associated with the uncompensated resistance and interfacial capacitance (*RC*) time constant of the cell were deconvoluted in the frequency domain. The flux of electron injection was described in terms of a competition between the relaxation of the porphyrin excited state and the electron transfer step. Experimental results in the presence of ferrocene and diferrocenylethane confirmed that as the Galvani potential difference is increased, the phenomenological electron transfer rate constant increases and the ZnTPPC coverage at the liquid/liquid junction decreases. Furthermore, the recombination rate constant decreases with increasing potentials, while the product separation rate constant did not show a clear potential dependence. Photocurrent studies were extended to the electron donors dimethylferrocene and trianisylamine, as well as to the electron acceptor tetracyanoquinodimethane. The results obtained clearly indicate that the Gibbs energy of activation for the charge transfer process is affected by the Galvani potential difference. It is suggested that the electron transfer dynamics are dependent on the local electric field generation by the specifically adsorbed ZnTPPC. The general expressions for the frequency dependent photocurrents at liquid/liquid interfaces are also introduced.

1 Introduction

In previous reports, we have described the photoelectrochemical responses originating from heterogeneous electron transfer reactions between photo-excited water soluble zinc porphyrins and hydrophobic quenchers at the water/1,2-dichloroethane (DCE) interface.[1,2] The dynamics and potential dependence of the photoresponses indicated that the electron transfer (ET) step is in competition with the relaxation of the excited state. Following the ET event, the intermediate ion pair can undergo a final product separation or back electron transfer. Due to the interfacial nature of this intermediate, back electron transfer involves a faradaic response of opposite sign to the initial photocurrent signal. In fact, these responses resemble the charge transfer–recombination behaviour familiar from illuminated semiconductor/electrolyte junctions.[3,4] The photoinduced ET as well as the recombination kinetics are dependent on the Galvani potential difference. Although the nature of this dependence is not clear yet, it was proved that the increment of the photocurrent with increasing applied potential involving zinc tetrakis(carboxyphenyl)porphyrin (ZnTPPC) and ferrocene was not determined by concentration polarisation phenomena.[2,5–7]

In addition to the dynamics of charge transfer between sensitisers and quenchers, responses associated with the charge/discharge of the interfacial double layer can also affect photo-transient measurements. In this sense, intensity modulated photocurrent spectroscopy (IMPS) is an ideal tool for deconvoluting the contribution of the various photoprocesses in the frequency domain.[4,8–12] This technique features a sinusoidal light perturbation superimposed to a constant bias light, and the ac-photocurrent is measured as a function of the frequency of illumination. In the present report, the kinetics of product separation and back electron transfer are studied by IMPS at various Galvani potential differences. The experimental results strongly suggest that the potential dependence of the phenomenological ET and recombination rate constants are linked to local potential perturbations introduced by the specifically adsorbed ZnTPPC.

† Part I; ref. 2

2 Theory

The elementary steps involved in the heterogeneous photooxidation of a species Q by a sensitiser S can be generally described as,

$$S_w \xrightarrow{h\nu} S_w^* \quad \text{Photoexcitation} \quad (1)$$

$$S_w^* \xrightarrow{k_d} S_w \quad \text{Decay of the excited state} \quad (2)$$

$$S_w^* + Q_0 \xrightarrow{k_{et}} [S^- \cdots Q^+]_{int} \quad \text{Electron transfer} \quad (3)$$

$$[S^- \cdots Q^+]_{int} \xrightarrow{k_{ps}} S_w^- + Q_0^+ \quad \text{Product separation} \quad (4)$$

$$[S^- \cdots Q^+]_{int} \xrightarrow{k_{rec}} S_w + Q_0 \quad \text{Recombination} \quad (5)$$

where the subindexes "w", "o" and "int" correspond to the aqueous, organic and interfacial regions respectively. According to our previous studies involving ZnTPPC,[2] the pseudo first order rate constant of electron transfer k_{et} is of the same order of the decay of the excited states k_d, *i.e.* 10^4–10^5 s^{-1} at potentials close to the point of zero charge (pzc). The time

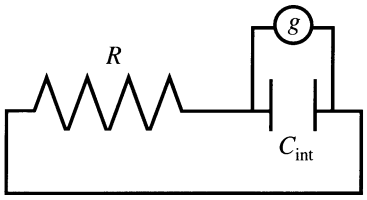

Fig. 1 Simplified equivalent circuit of the illuminated liquid/liquid interface under potentiostatic conditions.

scale of these processes is several orders of magnitude faster than the relaxation associated with the produce separation and recombination steps, which appear at hundreds of milliseconds. This difference in time scales allows one to separate the kinetics of processes (2) and (3), which determine the flux of electron injection, from the kinetics of $[S^-\cdots Q^+]_{int}$ disappearance.

The differential equations for the surface density of the sensitiser excited state Γ_s^* is given by,

$$d\Gamma_s^*/dt = I\sigma\Gamma_s - (k_{et} + k_d)\Gamma_s^* \quad (6)$$

where Γ_s is the surface density of the ground state, I is the photon flux and σ is the optical capture cross section. On the reductive quenching of ZnTPPC by ferrocene, two potential dependent parameters determine the electron injection flux: (i) the sensitiser coverage at the liquid/liquid junction and (ii) the electron transfer rate constant.[2] The surface coverage was found to be weakly dependent on the Galvani potential difference ($\Delta_o^w\phi$), following a Langmuir behaviour for anionic species. On the other hand, k_{et} exhibited a Tafel potential dependence near the pzc. While the coverage of porphyrin decreases with increasing $\Delta_o^w\phi$, the electron transfer rate constant increases. Considering the potential dependence of Γ_s and k_{et}, and assuming quasi-steady state conditions for steps

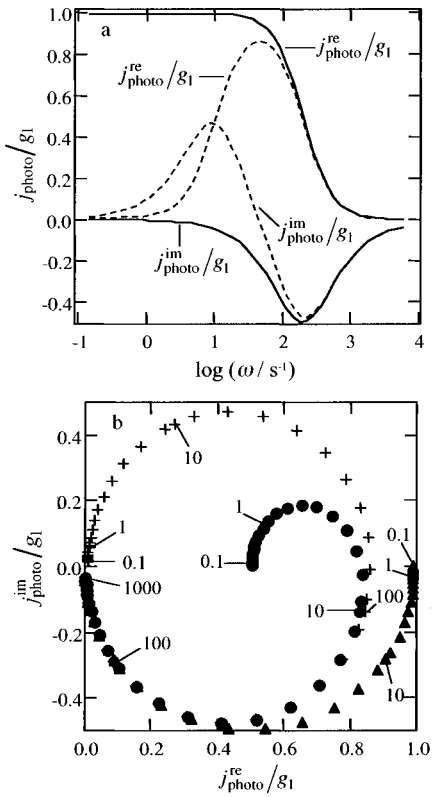

Fig. 2 Bode (a) representation of the normalised frequency dependent photocurrent with respect to g_1 as evaluated from eqns. (17) and (18). The RC_{int} constant was taken as 5×10^{-3} s^{-1}, while $k_{ps} = 0.1$ s^{-1} and $k_{rec} = 10$ s^{-1} (dashed line) and $k_{ps} = 10$ s^{-1} and $k_{rec} = 0.1$ s^{-1} (solid line). Complex representation of the IMPS responses (b), taking $k_{ps} = 0.1$ s^{-1} and $k_{rec} = 10$ s^{-1} (+), $k_{ps} = 10$ s^{-1} and $k_{rec} = 10$ s^{-1} (●), $k_{ps} = 10$ s^{-1} and $k_{rec} = 0.1$ s^{-1} (▲).

(1)–(3), it follows that the photoresponse associated with the flux of electron injection g is given by,[2]

$$g = ek_{et}\Gamma_s^* = ek_{et}\frac{I\sigma}{k_{et} + k_d}\Gamma_s \quad (7)$$

where

$$\Gamma_s = AN_s/(1 + A) \quad (8)$$

$$A = \left(\frac{a_{ZnTPPC^{z-}}}{a_{H_2O}}\right)\exp(-\Delta G_{ads}/RT)\exp(zbF\Delta_o^w\phi/RT) \quad (9)$$

and

$$k_{et} = k'_{et}\exp(\alpha F\Delta_o^w\phi/RT) \quad (10)$$

N_s is the maximum surface density of porphyrins, b is the fraction of the Galvani potential difference operating in the aqueous side and k'_{et} is the electron transfer rate constant at $\Delta_o^w\phi = 0$. Eqn. (10) implicitly assumes the presence of a monotonous potential distribution across the interface, which is not necessarily the case in the presence of adsorbed porphyrins. From eqn. (7), the parameter g exhibits a maximum as a result of the concurrent drop of the surface coverage and the increase of k_{et} with increasing potentials. The parameter g can be considered analogous to the flux of minority carriers determined by the Gärtner expression familiar from semiconductor photoelectrodes.[4,13,14] From the experimental point of view, the determination of g beyond the pzc, *ca.* 0.2 V, is severely complicated by the steep rise of the interfacial capacitance, leading to RC relaxation in the millisecond time scale.[2]

IMPS provides an alternative for deconvoluting the time constant of the various processes involved in the photoelectrochemical reaction. The charge distribution across the liquid/liquid interface can be generally described in terms of the uncompensated resistance R and the interfacial capacitance C_{int} as shown in Fig. 1. The flux of electron injection g [eqn. (7)] introduces an excess charge at the interface, which is relaxed *via* R. From this scheme and introducing steps (4) and (5) three further differential equations can be established under potentiostatic conditions,

$$d\Gamma_{[S^-\cdots Q^+]_{int}}/dt = k_{et}\Gamma_s^* - (k_{rec} + k_{ps})\Gamma_{[S^-\cdots Q^+]_{int}} \quad (11)$$

$$dq_{int}/dt = g - j_{ph} - ek_{rec}\Gamma_{[S^-\cdots Q^+]_{int}} \quad (12)$$

and

$$q_{int}/C_{int} = j_{ph}R \quad (13)$$

where q_{int} and j_{ph} stand for the interfacial excess charge and the photocurrent density respectively. Eqn. (11) corresponds to the time dependence of the ion pair surface density ($\Gamma_{[S^-\cdots Q^+]_{int}}$), while eqns. (12) and (13) describe the excess charge relaxation and the potentiostatic condition. In the presence of a periodic photon flux perturbation of frequency ω,

$$I = I_0 + \tilde{I} = I_0 + I_1\exp(i\omega t) \quad (14)$$

the frequency dependent concentration of the intermediate ion pair can be obtained from eqn. (11) as

$$(\Gamma_{[S^-\cdots Q^+]_{int}})_1 = k_{et}\left(\frac{I_1\sigma\Gamma_s}{k_{et} + k_d + i\omega}\right)\left(\frac{1}{k_{rec} + k_{ps} + i\omega}\right) \quad (15)$$

Finally, it follows from eqns. (12), (13) and (15) that the ac component of the photocurrent is given by

$$j_1 = g_1\frac{k_{ps} + i\omega}{k_{rec} + k_{ps} + i\omega}\left(\frac{1}{1 + RC_{int}i\omega}\right) \quad (16)$$

where

$$g_1 = k_{et}\left(\frac{I_1\sigma\Gamma_s}{k_{et} + k_d + i\omega}\right) \quad (17)$$

For low frequencies, $\omega \ll k_{et} + k_d$, g_1 behaves like a scaling factor at a given potential and light intensity. Under these conditions, eqn. (10) has the same form as the general IMPS expression for semiconductor electrodes when the interfacial capacitance is determined by the semiconductor space charge region.[15,16] The frequency dependent photocurrent normalised with respect to g_1 can also be expressed in terms of the real and quadrature components as,

$$\frac{j^{re}_{photo}}{g_1} = \frac{k_{ps}(k_{ps} + k_{rec}) - \omega^2(k_{rec} RC_{int} + 1)}{(k_{ps} + k_{rec} - RC_{int}\omega^2) + [(k_{ps} + k_{rec} + 1/RC_{int})RC_{int}\omega]^2} \quad (18)$$

and

$$\frac{j^{im}_{photo}}{g_1} = \frac{\omega\{k_{rec} - [k_{ps}(k_{ps} + k_{rec}] - \omega^2)RC_{int}\}}{(k_{ps} + k_{rec} - RC_{int}\omega^2) + (k_{ps} + k_{rec} + 1/RC_{int})RC_{int}\omega]^2} \quad (19)$$

In Fig. 2a, the normalised real and imaginary components of the photocurrent as a function of ω are contrasted for the limiting cases $k_{ps} \gg k_{rec}$ and $k_{ps} \ll k_{rec}$. For negligible recombination (solid line), the low frequency limit of j^{re}_{photo}/g_1 approaches unity, while only negative values of the imaginary part are obtained. Under strong recombination conditions, the low frequency limit of j^{re}_{photo}/g_1 is zero, and j^{im}_{photo}/g_1 exhibits a maximum as the frequency is increased. Complex representations of eqns. (18) and (19) are also displayed in Fig. 2b, where the familiar semicircles in the upper and lower quadrants are observed. Effectively, the low frequency response is determined by the competition between k_{ps} and k_{rec}, while the RC_{int} time constant dominates at higher frequencies. Fig. 2b also shows that for typical values of RC_{int}, the frequency range available for kinetic studies extends to less than 1 kHz. Within this frequency range, the quasi-steady approximation for the flux of electron injection is readily valid.

3 Experimental

All electrolyte solutions were prepared from analytical grade reagents. The supporting electrolyte in the organic phase was bis(triphenylphosphoranylidene) ammonium tetrakis(pentafluorophenyl)borate (**BTPPATPFB**). This electrolyte was prepared by metathesis of **BTPPACl** and **LiTPFB** in 2 : 1 mixtures of methanol and water, followed by recrystallisation in acetone. All other electrolyte solutions were prepared as previously reported.[1,2]

The electrochemical cell is displayed in Fig. 3. A three compartment cell was employed for all experiments, where the two reference electrodes were placed in separate compartments provided of luggin capillaries. The surface area of the liquid/liquid junction was 1.53 cm^2. The typical uncompensated resistance between the two reference electrodes was *ca.* 100 Ω. The interface was polarised *via* a custom built four electrode potentiostat in conjunction with a waveform generator Hi Tek PPR1. The Galvani potential difference was estimated from the formal transfer potential for tetramethylammonium, which corresponds to $\Delta^w_o\phi^{0\prime} = 0.160$ V.[17]

Photocurrent measurements were carried out with a He–Cd laser at 442 nm (Omnichrone). The interface was illuminated either in total internal reflection from the organic phase (with an incident angle of 75°) or perpendicularly to the liquid/liquid junction. As described previously, the photoresponses

Ag	Ag_2SO_4	Li_2SO_4 0.01 M Na_4 ZnTPPC water	BTPPATPFB 0.01 M quencher 10^{-3} M DCE	BTPPACl 0.001 M LiCl 0.01 M water	AgCl	Ag'

Fig. 3 Schematic representation of the electrochemical cell.

arise from adsorbed porphyrin species, therefore the photocurrent density is effectively independent of the angle of illumination.[1,2] For both illumination angles, the reference electrodes are kept in the dark avoiding any possible photopotential interference.[18] A photomultiplier tube (PMT) was employed for monitoring the light intensity either by transmission or reflection from the liquid/liquid junction. Photocurrent–potential curves under chopped illumination were recorded with a lock-in amplifier SR830 from Standford Research. IMPS spectra were carried out with an Acousto-Optic Modulator 1205C-2 from Isomet in conjunction with a Solartron 1250 frequency response analyser. The modulation frequency was swept from 0.1 mHz up to 1 kHz. The output of the PMT was employed as the phase reference. Low illumination levels were used in order to avoid photocurrent transients associated with the diffusion of the excited state. Under the present conditions, diffusion effects are observed at photocurrent densities higher than 5×10^{-7} A cm^{-2}. This rather low photocurrent density obliges the use of low photon fluxes and a light modulation depth in the range 50–80%. Despite the high modulation depth, the IMPS signal did not show distortions connected to higher harmonics of the ac photocurrent.

4 Results and discussion

4.1 Photocurrent–potential curves associated with the reductive quenching of ZnTPPC

Photocurrent–potential curves under chopped illumination at 12 Hz in the presence of diferrocenylethane (DFcET), ferrocene (Fc), dimethylferrocene (DMFc) and trianisylamine (TAA) are contrasted in Fig. 4. The increase of the in-phase component of the photocurrent j^{re}_{photo} with increasing applied potential is consistent with the potential dependence of k_{et} introduced in eqn. (10). On the other hand, the quadrature component j^{im}_{photo} does not feature the strong negative response observed in our previous analysis of the ferrocene derivatives.[2] The origin of this phase shift was related to the photo-

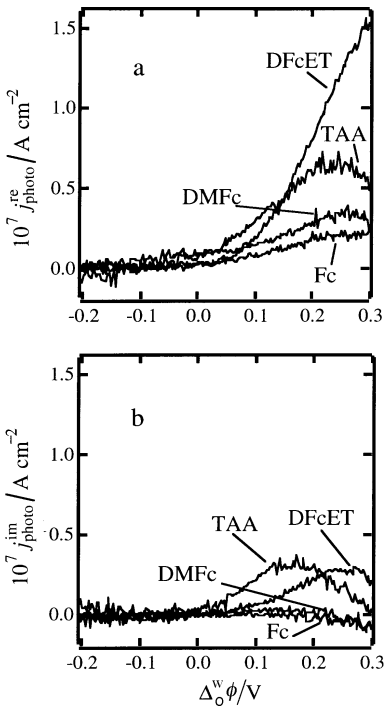

Fig. 4 Real (a) and quadrature (b) component of the photocurrent in the presence of diferrocenylethane (DFcFT), trianisylamine (TAA), dimethylferrocene (DMFc) and ferrocene (Fc). Illumination was chopped at 12 Hz, with an amplitude of 1.1×10^{16} cm^{-2} s^{-1} at $\lambda = 442$ nm.

oxidation of tetrakis(4-chlorophenyl)borate ($TPBCl^-$) which was present as the supporting electrolyte anion. By contrast, $TPFB^-$ exhibits a higher redox stability[18] and no photocurrent responses are observed in the absence of the neutral quenchers. The behaviour of j^{im}_{photo} at this frequency provides information on the recombination dynamics and the effects of the RC_{int} time constant.

For the present series of quenchers, DFcET exhibits the highest photocurrent density at positive potentials. Assuming that the potential dependence of k_{et} is similar for all quenchers, the differences observed in the real component of the photocurrent j^{re}_{photo} are related to the parameter k'_{et}. In the particular case of DFcET, it should also be considered that the overall concentration of ferrocenyl groups is twice as large as for the other ferrocene derivatives, which may account for part of the difference observed in the photocurrent densities. An interesting behaviour in Fig. 4 is that all electron donors exhibit very similar photocurrent onset potentials *i.e.* between -0.10 and 0.00 V. As discussed later, these results suggest that the dynamics of ET are not only determined by redox properties of the quencher but also by the interfacial behaviour of ZnTPPC.

The redox potentials of the various quenchers as well as the ground and excited states of the porphyrin are summarised in Table 1. In the case of the organic phase quenchers, potentials were measured by cyclic voltammetry on a 25 μm diameter ultramicroelectrode in a DCE solution containing $BTPPAPF_6$ as supporting electrolyte. The redox potentials were determined with respect to the ferrocene couple in the same electrolyte. $E^{DCE}_{Fc/Fc+}$. These data were also rescaled with respect to the potential in the aqueous phase, following previous reports by Cunnane *et al.*[19] Redox potentials for ZnTPPC were taken from ref. 20. According to the difference in redox potentials between the excited state of the porphyrin and the organic phase quenchers, photoinduced ET is thermodynamically favoured at all potentials within the experimental range. Furthermore, the thermodynamic driving force for the ET process is higher for DMFc and DFcET than for the other quencher species. However the results in Fig. 4 show photocurrent responses only at positive $\Delta^w_o\phi$, and the trend expected from the thermodynamic point of view fails to describe the experimental dependence of the photocurrent on the redox potential of the quencher.

The positive j^{im}_{photo} in the presence of DFcET reveals back-electron transfer at the frequency of illumination.[2] Photoresponses for TAA also exhibits a phase shift associated with the recombination step. On the other hand, photocurrents in the presence of DMFc and Fc appear almost in phase at all potentials. The absence of the recombination phase shift at 12 Hz does not formally imply that k_{rec} for DMFc and Fc is smaller than for DFcET or TAA. The recombination step effectively competes with product separation, therefore it is difficult to rationalise from a single frequency analysis whether the difference in recombination responses are brought about by k_{ps} or k_{rec}. In the following section, this analysis is extended to the whole frequency range available for the cases of Fc and DFcET.

Table 1 Redox potentials for the quenchers and ZnTPPC. Data regarding the organic phase quencher were obtained by cyclic voltammetry on a Pt ultramicroelectrode in DCE (see text)

Redox couple	$E^{DCE}_{Fc^+/Fc}$/V	E_{NHE}/V
Fc^+/Fc	0.00	0.40
$DFcET^+/DFcET$	−0.09	0.31
$DFcET^{2+}/DFcET^+$	0.07	0.47
$DMFc^+/DMFc$	−0.09	0.31
TAA^+/TAA	0.12	0.52
$TCNQ/TCNQ^-$	−0.35	0.05
$ZnTPPC^{4-}/ZnTPPC^{5-}$	—	−0.44[a]
$ZnTPPC^{3-}/ZnTPPC^{4-}$	—	1.18[a]
$ZnTPPC^{*4-}/ZnTPPC^{5-}$	—	1.19[a]
$ZnTPPC^{3-}/ZnTPPC^{*4-}$	—	−0.45[a]

[a] From ref. 20.

4.2 IMPS analysis in the presence of ferrocene and diferrocenylethane

IMPS spectra associated with the photo-oxidation of Fc and DFcET were analysed in the range 0.20–0.40 V. Typical spectra recorded in the presence of DFcET are displayed in Fig. 5. The illumination was introduced by total internal reflection (TIR) from the organic phase. From Figs. 5a and b, it is observed that the responses originating from the product separation–recombination competition and the RC_{int} time constant develop within the range 0.1–100 Hz. For both quenchers, a very slight shift of the low frequency limit toward higher photocurrent occurs as the Galvani potential difference is increased. On the other hand, the frequency of maximum imaginary part and the maximum value of j^{re}_{photo} follows a rather more complicated behaviour due to the different potential dependence of g_1, k_{ps}/k_{rec} and RC_{int}. Despite the low frequency scattering, the complex representation of IMPS data

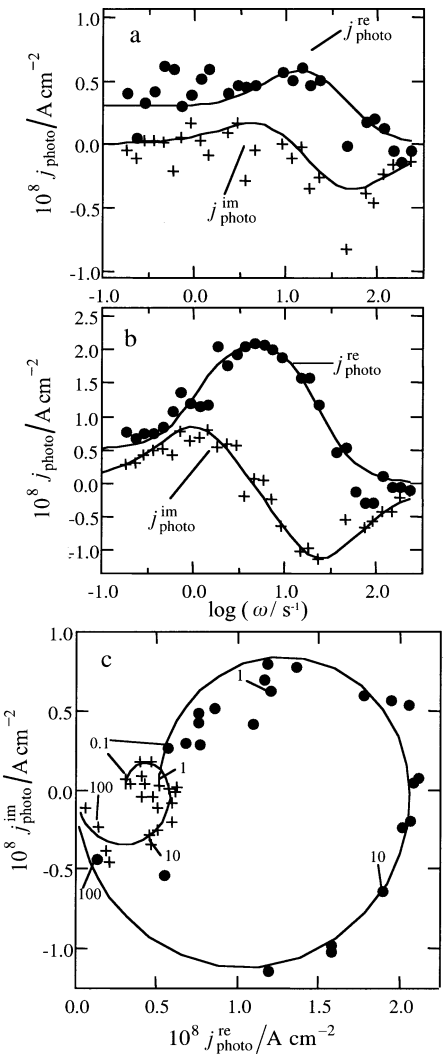

Fig. 5 Real and imaginary component of the intensity modulated photocurrent as a function of frequency in the presence of DFcET at 0.160 (a) and 0.310 V (b). Complex representation (c) of the IMPS data at 0.160 (+) and 0.310 (V) (●). The dc bias light was 4.5×10^{15} $cm^{-2}\,s^{-1}$ with a modulation depth of 80%. Solid lines correspond to the fitting of eqns. (17)–(18), taking g_1, k_{ps} and k_{rec} as adjustable parameters.

in Fig. 5c describes the semicircles in the upper and lower quadrants. In the case of Fc, the upper quadrant responses were observed at a very narrow potential range and at frequencies below 5 Hz. These results are consistent with the photocurrent potential curves shown in Fig. 4, where no positive quadrature components are observed at 12 Hz.

In order to assess g_1 as well as k_{ps} and k_{rec} as a function of $\Delta_o^w\phi$, eqn. (16) was fitted to the IMPS spectra recorded for both quenchers. The RC_{int} time constant was evaluated from impedance measurements carried out in the dark. The potential dependence of the RC_{int} time constant is shown in Fig. 6. A minimum value is observed close to 0.20 V, which is consistent with capacitance measurements previously reported.[2] The positive shift of the pzc in comparison to the water/DCE interface in the absence of ZnTPPC come as a result of the specific adsorption of porphyrin species. A non-linear least squares routine was employed for the fits of the IMPS spectra, where g_1, k_{ps} and k_{rec} were the adjustable parameters. Fittings consistently converged within the experimental frequency range, as exemplified in Fig. 5.

The potential dependence of g_1 obtained from the IMPS analysis in the presence of DFcET and Fc is displayed in Fig. 7. Both quenchers developed a maximum g^{max} within the potential range studied. As mentioned previously, g^{max} comes as a result of the decrease in Γ_s and the increase of k_{et} with increasing applied potentials. In the presence of Fc, g^{max} occurs at potentials slightly more positive than in the case of DFcET. The solid lines displayed in Fig. 7 indicate that the behaviour of g_1 can be phenomenologically described in terms of eqn. (7)–(10). For these fittings, ΔG_{ads} was taken as -41 kJ mol^{-1}, k_d as 10^5 s^{-1}, σ as 10^{-17} cm^2 and N_s as 5×10^{13} cm^{-2}.[2] The adjusting parameters were k'_{et}, α and b. The analysis of both curves resulted in common values for $b = 0.09 \pm 0.02$ and $\alpha = 0.4 \pm 0.1$. On the other hand, the differences arising between g_1 for DFcET and Fc are associated with the magnitude of the electron transfer rate constant k'_{et}. In the case of DFcET, the rate constant corresponds to $k'^{DFcET}_{et} = 612 \pm 63$ s^{-1}, while for Fc it was found $k'^{Fc}_{et} = 108 \pm 8$ s^{-1}. The fundamental aspects behind this difference in the electron transfer dynamics are still under investigation. As mentioned previously, the difference in redox potential (Table 1) is not the only determining factor in the electron transfer rate. An essential parameter for the calculation of the Gibbs energy of activation is also the potential drop across the planes where excited state and quencher are located during the ET step.[5,21–24] This parameter is rather difficult to estimate due to local perturbations introduced by specific adsorption and interfacial ion pairing involving the charged porphyrins.[2] Furthermore, difference in the quencher hydrophilicity can change the distance between the reaction planes.

IMPS analysis also reveals some insights into the dependence of k_{ps} and k_{rec} on the quencher and applied potential. Fig. 8 contrasts the rather weak dependence of k_{ps} with the exponential decrease of k_{rec} with increasing $\Delta_o^w\phi$. It is also observed that k_{rec} is similar for both quenchers within the same potential range. This rather surprising result indicates that the stronger recombination responses observed in the presence of DFcET arise from a slower product separation rather than a faster back-electron transfer. Specific properties such as charge, geometry, hydrophilicity, adsorption properties and molecular orientation of the photoinduced ion pairs can be involved in the dynamics of product separation.[25–27] However, the differences observed in the kinetics of product separation for the various quenchers are relatively small and difficult to rationalise in terms of these types of properties.

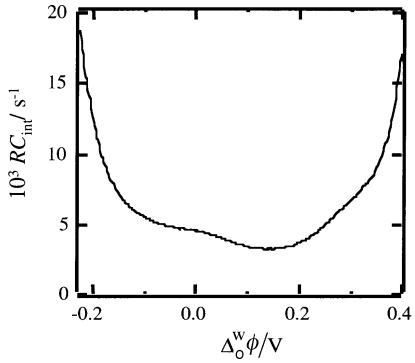

Fig. 6 RC_{int} time constant as a function of the Galvani potential difference obtained from impedance measurements in the absence of organic phase quenchers. A single RC_{int} time constant (Fig. 2) was employed for the analysis from 1 to 1000 Hz.

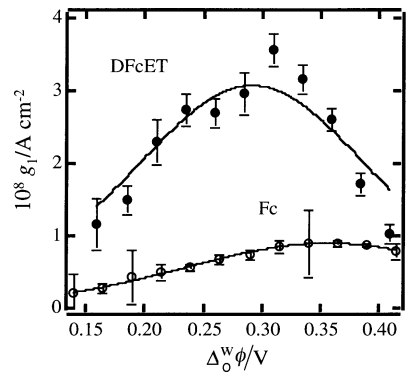

Fig. 7 Frequency dependent electron injection flux for DFcET and Fc as a function of the Galvani potential difference. Data were extracted from the IMPS analysis as exemplified in Fig. 6. Fittings to eqn. (7) are also displayed as solid lines. It was found that $\alpha = 0.4 \pm 0.1$ and $b = 0.09 \pm 0.02$ for both curves. Fits also provided a value for $k'^{DFcET}_{et} = 612 \pm 63$ s^{-1} and $k'^{Fc}_{et} = 108 \pm 8$ s^{-1}.

4.3 Further comments on the potential dependence of k_{et} and k_{rec}

IMPS analysis for Fc and DFcET showed an exponential decrease of k_{rec} with increasing $\Delta_o^w\phi$ (Fig. 8). Assuming that the behaviour of k_{rec} is connected to changes in the Gibbs

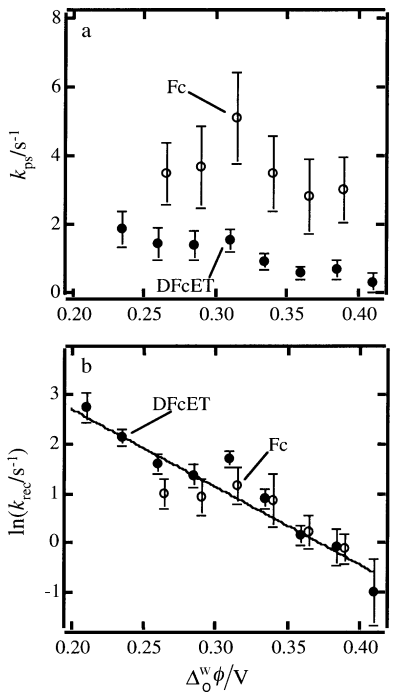

Fig. 8 Potential dependence of k_{ps} (a) and k_{rec} (b) as obtained from IMPS analysis in the presence of DFcET and Fc. The weak dependence of k_{ps} contrasts with the exponential decrease of k_{rec} with increasing $\Delta_o^w\phi$.

activation energy for recombination ($\Delta G^{\ddagger}_{rec}$), the potential dependence of k_{rec} and k_{et} are intrinsically correlated. In other words, if the activation energy for the photoinduced ET step ($\Delta G^{\ddagger}_{et}$) is decreased, then $\Delta G^{\ddagger}_{rec}$ is increased. This correlation is graphically described in Fig. 9. It should be considered that although recombination consists in an ET from the sensitiser back to the electron donor, it does not correspond to the reverse process of the photoinduced step. As shown in Fig. 9, the initial state of the ET process involves the sensitiser excited state, while the recombination products are the ground state sensitiser and the reduced electron donor. From simple geometric arguments, it is deduced that the phenomenological transfer coefficient associated with the recombination potential dependence is equivalent to the transfer coefficient α introduced in eqn. (10), but with opposite sign. This relation stands if the solvent reorganisation term involving the excited state and the ground state of the sensitiser are similar. Considering that neither changes in the structure nor in the interfacial behaviour of the porphyrin occur upon excitation, the reorganisation energy term should be equivalent for both states.[21–24,28] Consequently, it follows

$$k_{rec} = k'_{rec} \exp(-\alpha F \Delta^{w}_{o} \phi / RT) \quad (20)$$

As for eqn. (10), it should be noted that implicit assumptions regarding the potential distribution are made, *i.e.* only monotonous potential profiles are considered. In the case of liquid/liquid interfaces, α may also represent the fraction of the applied potential difference which is effective in the interfacial reaction layer and may have a different meaning than the classical one associated with the Butler–Volmer mechanism illustrated in Fig. 9. The exponential dependence in Fig. 8 provides a value of $\alpha = -0.4 \pm 0.1$, which is consistent with the analysis of g_1 as a function of the applied potential (see Fig. 7). The correlation of the potential dependence of k_{et} and k_{rec} support the link between the Gibbs activation energies for the charge transfer processes ($\Delta G^{\ddagger}_{et}$ and $\Delta G^{\ddagger}_{rec}$) and the Galvani potential difference. Nevertheless, despite the consistent behaviour of k_{et} and k_{rec} with the applied potential for the ferrocene derivatives, photocurrent–potential relations in the presence of electron acceptors reveal a rather more complex picture than that depicted in Fig. 9.

Photocurrent–potential curves at various porphyrin concentrations in the presence of tetracyanoquinodimethane (TCNQ) are displayed in Fig. 10. By contrast to electron donor species, photocurrent responses are negative as the excited state injects an electron into the organic phase species.[1] j^{re}_{photo} strongly increases as $\Delta^{w}_{o}\phi$ becomes more negative, reaching a plateau in the range of 0.00 to -0.10 V. The negative j^{im}_{photo} also indicates the presence of back-electron transfer reaction. It is also observed that the dependence of the photocurrent on the bulk concentration of porphyrin is rather weak. As the coverage of porphyrins increases with decreasing potentials, the flux of electron injection becomes less dependent on the bulk concentration. In the case of electron donor species at positive potentials, the concentration dependence of the photocurrent is rather stronger due to the smaller coverage.[2] At potentials more negative than -0.10 V, a sharp increase of the photocurrent is also developed. However, this response occurs in the potential range of porphyrin transfer to the organic phase.

The potential independence of the photocurrent between 0.00 and -0.10 V for TCNQ and the common photocurrent onset potential for the electron donors suggest that the porphyrin coverage also plays a role in the dynamics of ET. It is expected that the specific adsorption of the negatively charged porphyrin generates an inversion of the local electric field which may affect the kinetics of interfacial electron transfer. As mentioned previously, the potential of minimum RC_{int} (Fig. 6) indicates an interfacial excess of negative charge which perturbs the local potential distribution. This negatively charged plane introduces an effective energy barrier for ET to the excited state. In principle, this energy barrier could be the reason behind the absence of photoresponses at negative potentials in the presence of electron donors, even if the ET processes are thermodynamically favourable. Consequently, as the porphyrin is desorbed, the local electric field becomes less negative and the ET to the excited state speeds up. Correspondingly, the increment of the photocurrent with decreasing $\Delta^{w}_{o}\phi$ in the case of TCNQ is only observed in the range where the porphyrin coverage is also dependent on the applied potential.

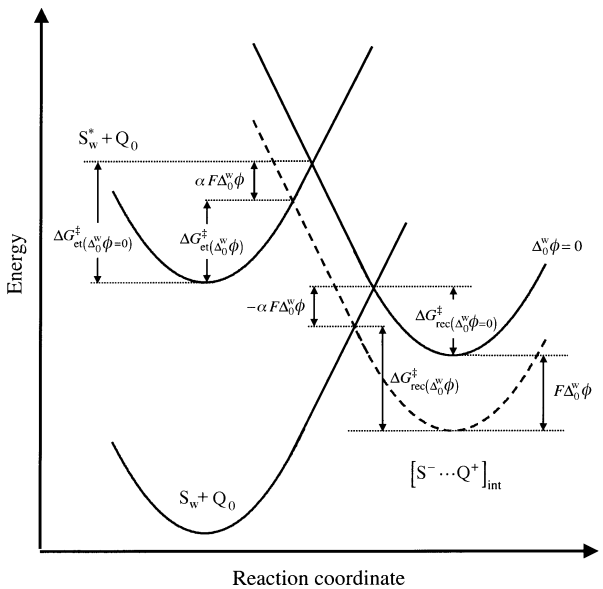

Fig. 9 Schematic representation of energy *vs.* reaction coordinate for the recombination process. Assuming the same reorganisation energy for the ground and excited state of porphyrin, the change in $\Delta G^{\ddagger}_{et}$ and $\Delta G^{\ddagger}_{rec}$ with $\Delta^{w}_{o}\phi$ is determined by the same transfer coefficient but with opposite sign.

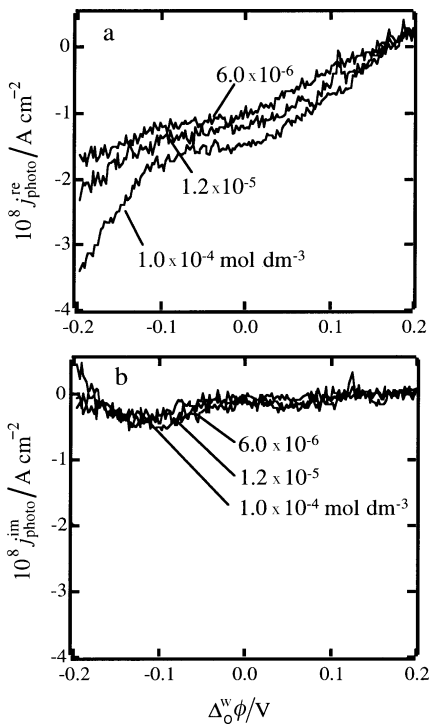

Fig. 10 Real (a) and quadrature (b) component of the photocurrent in the presence of TCNQ at various concentration of ZnTPPC. The experimental conditions were similar to those described in Fig. 5. However, there is some uncertainty in the photon flux arriving to the interface due to the absorption of TCNQ at 442 nm.

The apparent link between k_{et} and the local electric field suggests that phenomenological descriptions in terms of Tafel relations are not rigorously applicable over the whole potential range. A more quantitative description of the electron transfer dynamics as a function of the applied potential should address the interfacial charge distribution in the presence of the porphyrin species. Differential capacitance[2] and surface tension measurements[29] suggest that the excess charge arises not only from specific adsorption of ZnTPPC, but also from interfacial ion association.[30]

5 Conclusions

IMPS analysis associated with the heterogeneous quenching of ZnTPPC by ferrocene derivatives at the water/DCE interface allow the study of the dynamic photoresponses as a function of the Galvani potential difference. The contribution arising from the electron injection flux, the recombination–product separation competition and the RC_{int} time constant were deconvoluted in the frequency range 0.1–100 Hz. The fraction of the Galvani potential difference developed between the porphyrin adsorption plane and the bulk of the aqueous phase as well as phenomenological ET transfer coefficient were obtained from the potential dependence of the electron injection flux. It was concluded that the difference in the photoresponses associated with DFcET and Fc arises from different electron transfer and product separation rate constants.

Studies of the potential dependence of the electron transfer and recombination rate constants, complemented by photocurrent measurements for various quenchers, reveal a link between $\Delta G_{et}^{\ddagger}$ and $\Delta G_{rec}^{\ddagger}$ with the Galvani potential difference. For the porphyrin reductive quenching, the photocurrent onset potential was found to be independent of the electron donor species in the organic phase. This onset potential coincides with the potential at which the porphyrin coverage approaches unity, *i.e.* 0.0 V. By contrast, the photoreduction of TCNQ exhibits increasing photocurrents as $\Delta_o^w\phi$ becomes more negative, reaching a plateau between 0.00 and -0.10 V. The coincidence between the photocurrent onset potential for the reductive quenching and the photocurrent plateau for the oxidative quenching suggests that the electron transfer dynamics are affected by the local electric field associated with the specific adsorption of ZnTPPC.

Acknowledgements

The authors are grateful for financial support from the Fonds National Suisse de la Recherche Scientifique (project 2000-043381-95/1). We also acknowledge discussions with Paolo Galletto and technical assistance by Valérie Devaud. The Laboratoire d'Electrochimie is part of the European Network ODRELLI (Organisation, Dynamics and Reactivity at Electrified Liquid/Liquid Interfaces).

References

1 D. J. Fermín, Z. Ding, H. D. Duong, P.-F. Brevet and H. H. Girault, *Chem. Commun.*, 1998, 1125.
2 D. J. Fermín, Z. Ding, H. Duong, P.-F. Brevet and H. H. Girault, *J. Phys. Chem. B.*, 1998, **102**, 10334.
3 L. M. Peter, in *Photocatalysis and Environment*, ed. M. Schiavello, Kluwer Academic Publishers, London, 1988, p. 243.
4 L. M. Peter, *Chem. Rev.*, 1990, **90**, 753.
5 H. H. J. Girault and D. J. Schiffrin, *J. Electroanal. Chem.*, 1988, **244**, 15.
6 W. Schmickler, *J. Electroanal. Chem.*, 1997, **429**, 123.
7 Z. Ding, D. J. Fermín, P.-F. Brevet and H. H. Girault, *J. Electroanal. Chem.*, 1998, **458**, 139.
8 D. Vanmaekelbergh, A. R. Dewit and F. Cardon, *J. Appl. Phys.*, 1993, **73**, 5049.
9 D. J. Fermín, E. A. Ponomarev and L. M. Peter, in *Photoelectrochemistry*, ed. K. Rajeshwar, L. M. Peter, A. Fujishima, D. Meissner and M. Tomkiewich, The Electrochemical Society, Inc., Pennington, 1997, p. 62.
10 E. A. Ponomarev and S. D. Babenko, *J. Electroanal. Chem.*, 1994, **371**, 27.
11 G. H. Schoenmakers, D. Vanmaekelbergh and J. J. Kelly, *J. Phys. Chem.*, 1996, **100**, 3215.
12 A. R. de Wit, D. Vanmaekelbergh and J. J. Kelly, *J. Electrochem. Soc.*, 1992, **139**, 2508.
13 W. W. Gärtner, *Phys. Rev.*, 1959, **116**, 84.
14 Y. V. Pleskov and Y. Y. Gurevich, *Semiconductor Photoelectrochemistry*, Consultants Bureau, NY, 1986.
15 E. A. Ponomarev and L. M. Peter, *J. Electroanal. Chem.*, 1995, **396**, 219.
16 R. Peat and L. M. Peter, *J. Electroanal. Chem.*, 1987, **228**, 351.
17 Y. Shao, PhD Thesis, University of Edinburgh, Edinburgh, 1991.
18 A. R. Brown, L. J. Yellowlees and H. H. Girault, *J. Chem. Soc., Faraday Trans.*, 1993, **89**, 207.
19 V. J. Cunnane, G. Geblewicz and D. J. Schiffrin, *Electrochim. Acta*, 1995, **40**, 3005.
20 K. Kalyanasundaram, *Photochemistry of Polypyridine and Porphyrin Complexes*, Academic Press, London, 1992.
21 R. A. Marcus, *J. Phys. Chem.*, 1990, **94**, 4152.
22 R. A. Marcus, *J. Phys. Chem.*, 1990, **94**, 1050.
23 R. A. Marcus, *J. Phys. Chem.*, 1991, **95**, 2010.
24 Y. Cheng and D. J. Schiffrin, *J. Chem. Soc., Faraday Trans.*, 1993, **89**, 199.
25 P.-A. Brugger and M. Gratzel, *J. Am. Chem. Soc.*, 1980, **102**, 2461.
26 G. J. Kavarnos, *Fundamentals of photoinduced electron transfer*, VCH Publishers, Inc., New York, 1993.
27 I. R. Gould, J. E. Moser, B. Armitage and S. Farid, *Res. Chem. Intermed.*, 1995, **21**, 793.
28 H. H. Girault, *J. Electroanal. Chem.*, 1995, **388**, 93.
29 M. C. Martin, unpublished results.
30 C. M. Pereira, W. Schmickler, F. Silva and M. J. Sousa, *J. Electroanal. Chem.*, 1997, **436**, 9.

Paper 9/00142E